BMC Medicine

RESEARCH

Open Access

Retinomics: a window to multidisease prediction using retinal biomarkers from routine eye imaging

Mayinuer Yusufu[1,2], Matthew J. Burton[3,4], Shanshan Jin[5], Xianwen Shang[6,7,8,9*], Lei Zhang[1,10], Danli Shi[7,8,9*] and Mingguang He[7,8,9,11*]

Abstract

Background The aim of this study is to investigate the potential of retinal biomarkers (retinomics) derived from color fundus photography and optical coherence tomography for predicting multiple diseases.

Methods Using UK Biobank cohort data, we applied least absolute shrinkage and selection operator regression to address multicollinearity and identify key biomarkers. Cox proportional hazards models, with and without retinomic features. Detection rates (DR) across false positive rates (FPR: 5–40%) were assessed to ensure improved sensitivity without disproportionate false positives.

Results Three retinomic features emerged as top predictors: ganglion cell-inner plexiform layer (37 diseases), retinal pigment epithelium (33 diseases), and central subfield of inner segment/outer segment-RPE (32 diseases). Adding retinomics improved mean C-index from 0.653 to 0.693 (+6.4%) in baseline models (age and sex) and from 0.697 to 0.721 (+3.5%) in clinical models (traditional common risk factors). A simplified retinal model (retinomics + age/sex) achieved C-index ≥ 0.75 for 13 diseases. Retinomics enhanced prediction by > 5% for 24 diseases in baseline models and 12 diseases in clinical models. DR improvements across FPR ranges confirmed robust performance without excessive false positives.

Conclusions Retinomics universally enhanced disease prediction, with marked gains for conditions like cardiovascular and metabolic disorders. The onset of presbyopia (~ 50 years)—a common trigger for eye exams—aligns with escalating chronic disease risks, suggesting an opportunity to leverage routine eye care for broader health assessment. While requiring further validation, this approach demonstrates the potential to enhance health screening efficiency using existing ophthalmic infrastructure, offering particular value for resource-limited settings.

Keywords Retinal neural layers, Retinal vascular measurements, Neurovascular biomarkers, Cohort study, Retina-based microvascular health assessment system, Chronic diseases prediction, Preventive care

*Correspondence:
Xianwen Shang
xianwen.shang@polyu.edu.hk
Danli Shi
danli.shi@polyu.edu.hk
Mingguang He
mingguang.he@polyu.edu.hk
Full list of author information is available at the end of the article

Background

Early prediction of disease risk prior to clinical onset is critical for enabling timely interventions and improving patient outcomes. While traditional methods such as blood tests and imaging have advanced significantly, they remain largely confined to single-disease identification [1] and face limitations in scalability due to invasiveness, cost, and technical complexity. The emergence of omics technologies—high-throughput molecular profiling—has enabled comprehensive analyses of disease pathways [2, 3] with metabolomics and proteomics demonstrating potential for multi-disease risk prediction [4, 5]. However, these approaches are costly, often require specialized infrastructure and invasive sampling, hindering their integration into routine clinical care.

The retina, uniquely, offers a non-invasive window into systemic health, allowing direct visualization of both neural and microvascular structures [6] through widely accessible imaging modalities like color fundus photography (CFP) and optical coherence tomography (OCT). Our group previously developed the Retina-based Microvascular Health Assessment System-Fluorescein Angiography (RMHAS-FA) [7], a deep learning framework that automates segmentation of retinal vasculature. This system generates hundreds of intricate "vascular fingerprints" [8], quantifying retinal microarchitecture with unprecedented granularity. Furthermore, while prior work has uncovered multidimensional relationships between retinal vascular networks from CFP and neural layers from OCT [9], most research has focused on isolated CFP or OCT measurements [10, 11], neglecting the complementary insights offered by multimodal imaging. This presents a crucial gap where a comprehensive neurovascular retinomic approach—combining microvascular, macrovascular, and neural layer data across modalities—remains unexplored for multi-disease risk stratification. These features underpin "retinomics," an emerging discipline focused on large-scale biomarker discovery to link retinal phenotypes with systemic diseases such as cardiovascular disorders, diabetes, and neurodegeneration [12, 13].

More importantly, retinal screening aligns with a pivotal window for preventive care: routine eye exams, often initiated around age 50 due to presbyopia, coincide with the onset of elevated risk for chronic diseases. This alignment suggests that retinomics may have the potential to bridge ophthalmology and systemic health.

In this study, we leverage the UK Biobank [14], a large population-based cohort, to investigate the predictive value of neurovascular retinomics. By integrating CFP and OCT-derived features—encompassing large-medium vessels, capillaries, and neural layers—we aim to establish a multimodal framework for evaluating the potential of retinomics in stratifying risks of systemic conditions. Our work explores retinomics as a potential non-invasive tool for systemic health assessment, bridging critical gaps between single-modality studies and holistic risk prediction.

Methods

Study population

The study population was derived from the UK Biobank study, a prospective cohort study that recruited around 500,000 participants aged between 40 and 69 years at the baseline from 2006 to 2010 [14]. Ocular imaging including CFP and OCT was introduced in 2019 at six assessment centers [15]. The UK Biobank study received ethics approval from the North West Multi-Centre Research Ethics Committee (Ref 11/NW/0382) and obtained consent from participants at enrollment.

Inclusion and exclusion criteria

Participants who withdrew consent or lacked CFP/OCT data were excluded. Low-quality CFP images classified as "Reject" by RMHAS-FA [7] were removed. For OCT, quality control indicators generated by the Topcon 3D OCT-1000 Mark II system [15, 16] were applied. After matching OCT and CFP images by eye laterality, only the highest-quality pair per participant was retained. For each incident disease analysis, participants with prevalent disease at baseline were excluded, and for sex-specific conditions, people of the opposite sex were removed. The inclusion/exclusion processes for participants and image data at each stage of the selection process are shown in Fig. 1.

Retinomic profiling

Topcon 3D OCT-1000 Mark II system was used for retinal image acquisition [15]. The retinomic profiles consisted of retinal vascular features and retinal neural layer measurements. The measurements of large-medium vessels and capillaries were extracted from CFP using RMHAS-FA(7), including measurements of caliber, density, complexity, tortuosity, and branching angle. Details on the vascular measurements have been previously published [8]. The measurements of retinal neural layers were derived from OCT scans using Topcon Advanced Boundary Segmentation software [16]. Details can be found at https://biobank.ndph.ox.ac.uk/showcase/label.cgi?id=100016.

Outcomes

We included 63 chronic conditions as specified in the previous publication [17] and identified those conditions using the International Classification of Diseases, edition 10 (ICD-10) and ICD-9. Additional file 1: Tables

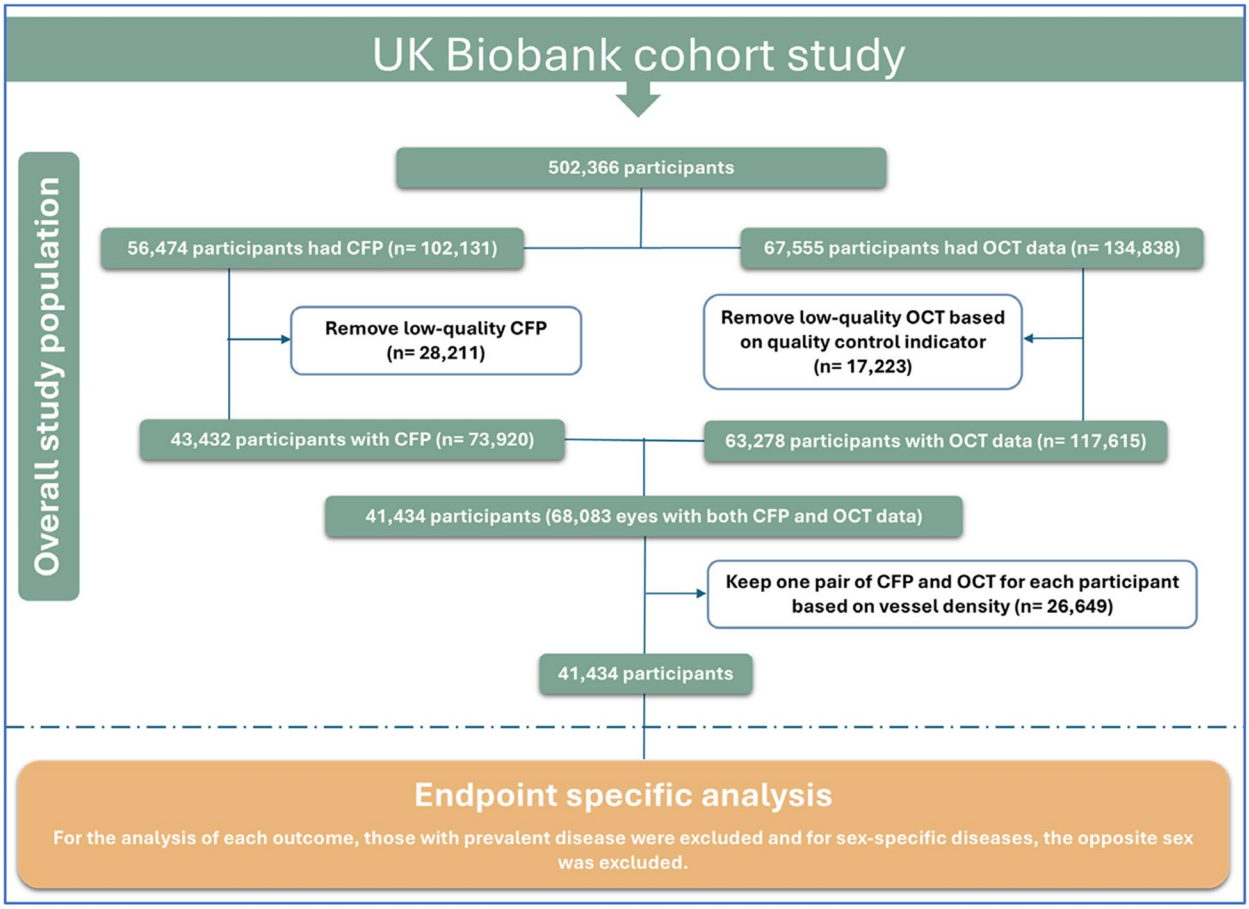

Fig. 1 Participants selection process. *OCT* optical coherence tomography, *CFP* color fundus photograph. N indicates the number of images

S1–S2 present the Field IDs and ICD codes used to identify prevalent and incident diseases. Follow-up starts on the date of the image acquisition and ends on the date of death, or incident outcomes, or October 31, 2022, whichever occurs first. We excluded those diseases with less than 30 incident events (the cut off was 15 for sex-specific diseases).

Statistical analysis

Retinal parameters with > 30% missing values were excluded, and outliers were removed following the method proposed by Zekayat et al. [18]. Remaining missing data were imputed using the multiple imputation by chained equations (MICE) package in R. After removing outliers, the distributions of all parameters were approximately normal upon visual inspection. All parameters were z-score standardized, which does not assume normality and ensures comparable scales across parameters for subsequent feature selection and predictive modeling.

The least absolute shrinkage and selection operator (LASSO) regression was used to identify retinomic biomarkers with predictive associations for each disease. LASSO's L1 regularization automatically excludes non-informative features by shrinking their coefficients to zero, ensuring only meaningful retinal biomarkers contribute to the predictive models. Prevalent cases for the corresponding outcome were excluded from the analysis, and sex-specific conditions were taken into consideration if applicable.

After feature selection, we fitted Cox proportional hazards models to assess the performance of 4 survival models in predicting incident diseases: (1) Baseline model: incorporating age and sex only; (2) Clinical model: age and sex along with clinical factors including body mass index (BMI), ethnicity, smoking status, alcohol consumption, and physical activity (well-established common modifiable risk factors for a wide range of diseases); (3) Retinal model: combining the baseline model and selected retinal features from LASSO regression; (4) Full model: combination of the clinical model and selected retinal features. Additional file 1: Table S3 shows the definitions of variables used in the current study.

The concordance index (C-index) was used to evaluate predictive performance. The C-index measures the probability that, for any randomly selected pair of subjects, the one with the higher predicted risk experiences the event earlier. We selected the C-index because it accounts for time-to-event information, making it more appropriate than traditional binary classification metrics for evaluating predictive models of chronic disease progression. In addition, to assess the statistical significance of improvements in model discrimination after adding retinal parameters, we employed the Likelihood Ratio Test (LRT) for each disease where we observed a > 5% improvement in C-index (either retinal model vs. baseline model, or full model vs. clinical model). Additionally, we calculated detection rate (DR) and false positive rate (FPR) to evaluate the models' screening capabilities and to assess the balance between correctly identifying disease cases while minimizing false alarms. We focused on the DR across FPR range of 5% to 40%, as this reflects the clinically practical operating range for predictive models. FPR values exceeding 40% would result in unacceptably high false positive rates, making such models unsuitable for real-world implementation. DR (proportion of affected people with a positive result) was defined by the number of true positives divided by the sum of the false negatives and the true positives. FPR (proportion of unaffected people with a positive result) was determined by the ratio of false positives to the sum of true negatives and false positives. We further assessed calibration using the Integrated Calibration Index (ICI), which measures how closely predicted risks match observed outcomes. Additional file 1: Fig. S1 shows the general design of current study and Fig. 2 illustrates the methodological framework of the analyses.

In addition, we investigated the predictive values of vascular and neural retinomics separately (Additional file 1: Figs. S2–S3) and model evaluation without LASSO feature selection (Additional file 1: Fig. S4). Further, we examined 5-year and 10-year predictions as sensitivity analyses (Additional file 1: Figs. S5–S6). All analyses were conducted using R Version 4.2.3 (Vienna, Austria).

Results

Characteristics of participants

The study included a total of 41,434 participants, comprising 22,898 (55.3%) females and 18,536 (44.7%) males. The mean age of the overall sample was 55.3 years (standard deviation [SD] 8.19). The mean BMI was 27.2 kg/m^2 (SD: 4.74), and physical activity levels were mostly moderate to high. Table 1 shows the details of the baseline characteristics of participants in the overall sample and by sex.

After excluding human immunodeficiency virus and anorexia due to insufficient incident cases (1 and 8 cases, respectively), 61 diseases were analyzed. The highest numbers of incident cases were observed in cardiometabolic conditions, with hypertension ($n = 4162$), high cholesterol ($n = 3334$), and coronary heart disease ($n = 2450$) being the most prevalent. Among musculoskeletal conditions, osteoporosis showed a high incidence ($n = 3259$), as did painful conditions ($n = 3111$). Gastrointestinal disorders were also common, with dyspepsia and diverticular disease accounting for 5084 and 4185 incident cases, respectively. For cancers, apart from other cancers ($n = 2341$), the most frequent were skin cancer ($n = 1461$), followed by prostate cancer ($n = 942$), and breast cancer ($n = 799$). Among neurological and mental health conditions, anxiety ($n = 1883$) and depression ($n = 1464$) showed the highest incidence. The least frequent conditions (excluding those already excluded) were polycystic ovary ($n = 16$), uterine/endometrial cancer ($n = 20$), and schizophrenia/bipolar disorder ($n = 37$). The details of disease incidence and follow-up period can be found in Additional file 1: Table S4.

Retinomic features selected for disease prediction

LASSO identified retinal parameters for all diseases except for schizophrenia/bipolar disorder, Meniere disease, and polycystic ovary, leaving 58 diseases included in the further analysis. Figure 3A shows the retinomic feature types selected with LASSO for the prediction of diseases and Fig. 3B shows the number of diseases where the retinal parameter was selected for prediction. Average ganglion cell inner plexiform layer thickness (GC-IPL), inner segment/outer segment—retinal pigment epithelium (ISOS-RPE) thickness of central subfield, and overall average RPE thickness, and were selected for 37, 33, and 32 diseases, respectively. Other neural retinal parameters selected for more than 20 diseases included average external limiting membrane-ISOS (ELM-ISOS) thickness, average retinal nerve fiber layer thickness (RNFL), ELM-ISOS thickness of outer subfield, ELM-ISOS thickness of central subfield, ISOS-RPE thickness of outer subfield, and average inner nuclear layer thickness (INL), while vascular retinal parameters selected for more than 20 diseases included width of non-terminal veins, venular curve angle, arterial vessel area density (VAD) in the macular region, venular VAD, the width of veins, venular VAD outside the macular region, number of arterial bifurcation and non-terminal arteries, venular branching angle, and arterial twist-based tortuosity. Additional file 1: Tables S5–S6 show the full list of selected retinomics and corresponding diseases, from the feature-centered and disease-centered perspectives, respectively. There were 11

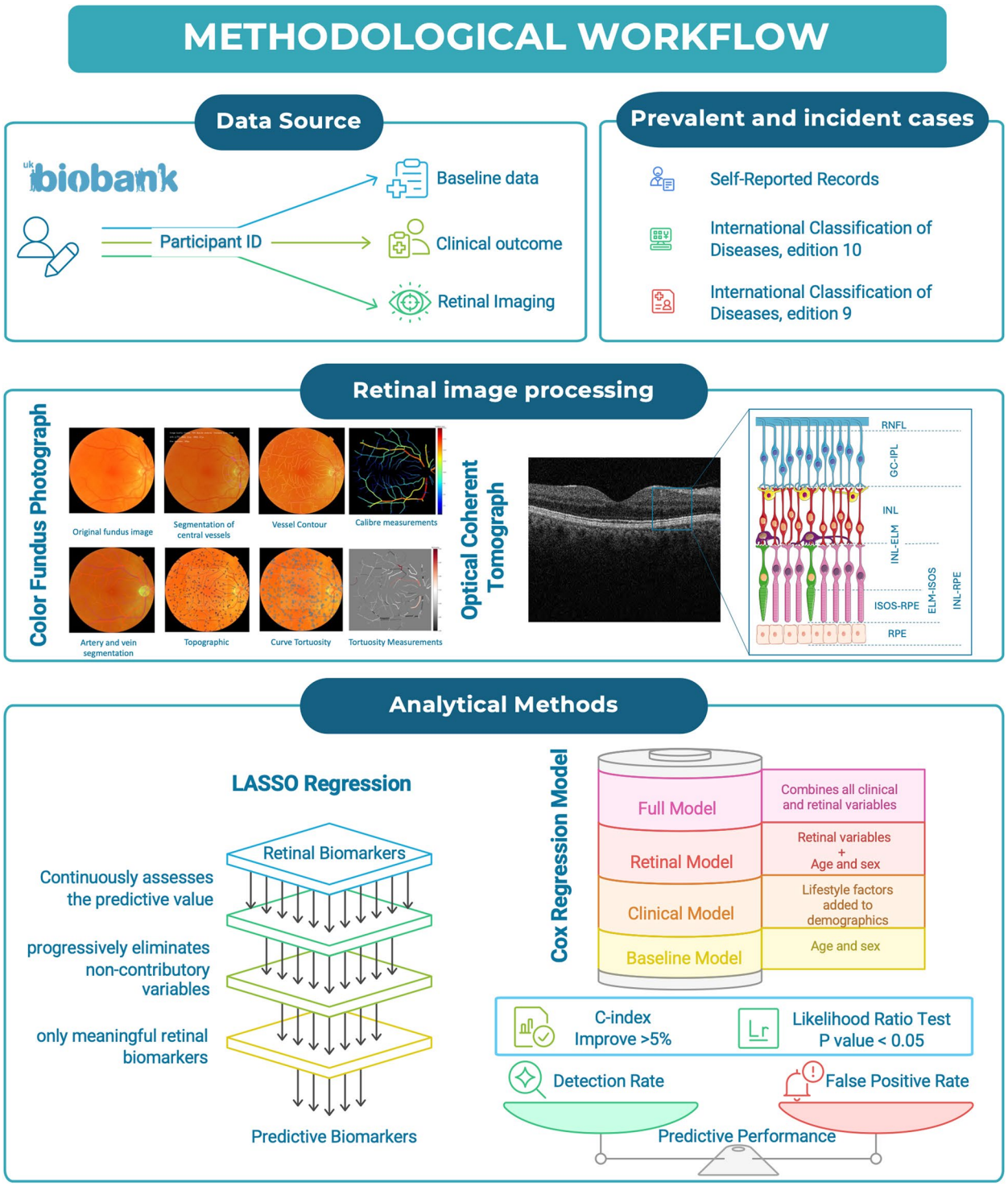

Fig. 2 Methodological framework for retinomics-based predictive modeling. This figure used image provided by Servier Medical Art (https://smart.servier.com/), licensed under CC BY 4.0 (https://creativecommons.org/licenses/by/4.0/) and from Chilton, J. (2020). Ependymal cell.Zenodo. https://doi.org/10.5281/zenodo.3926497 from SciDraw licensed under CC BY 4.0. *RNFL* retinal nerve fiber layer, *GC-IPL* ganglion cell layer-inner plexiform layer, *INL* inner nuclear layer, *ELM* external limiting membrane, *ISOS* inner segment/outer segment, *RPE* retinal pigment epithelium

Table 1 Baseline characteristics of participants

	All (*N* = 41,434)	Female (*N* = 22,898)	Male (*N* = 18,536)
Age (years)			
Mean (SD)	55.3 (8.19)	55.1 (8.05)	55.5 (8.35)
Education, *N* (%)			
High	15,098 (36.4%)	8082 (35.3%)	7016 (37.9%)
Intermediate	20,668 (49.9%)	11,777 (51.4%)	8891 (48.0%)
Low	5150 (12.4%)	2763 (12.1%)	2387 (12.9%)
Missing	518 (1.3%)	276 (1.2%)	242 (1.3%)
Smoking status, *N* (%)			
Never	23,376 (56.4%)	13,903 (60.7%)	9473 (51.1%)
Previous	13,769 (33.2%)	7001 (30.6%)	6768 (36.5%)
Current	4053 (9.8%)	1873 (8.2%)	2180 (11.8%)
Missing	236 (0.6%)	121 (0.5%)	115 (0.6%)
Drinking status, *N* (%)			
Never	1980 (4.8%)	1403 (6.1%)	577 (3.1%)
Previous	1429 (3.4%)	805 (3.5%)	624 (3.4%)
Current	37,870 (91.4%)	20,602 (90.0%)	17,268 (93.2%)
Missing	155 (0.4%)	88 (0.4%)	67 (0.4%)
Body mass index (kg/m^2)			
Mean (SD)	27.2 (4.74)	26.8 (5.14)	27.7 (4.13)
Missing, *N* (%)	212 (0.5%)	112 (0.5%)	100 (0.5%)
Physical activity, *N* (%)			
Low	5742 (13.9%)	2964 (12.9%)	2778 (15.0%)
Moderate	13,552 (32.7%)	7646 (33.4%)	5906 (31.9%)
High	13,764 (33.2%)	7077 (30.9%)	6687 (36.1%)
Missing	8376 (20.2%)	5211 (22.8%)	3165 (17.1%)
Overall health, *N* (%)			
Good/Excellent	30,465 (73.5%)	17,218 (75.2%)	13,247 (71.5%)
Fair	8931 (21.6%)	4603 (20.1%)	4328 (23.3%)
Poor	1775 (4.3%)	937 (4.1%)	838 (4.5%)
Missing	263 (0.6%)	140 (0.6%)	123 (0.7%)
SBP (mmHg)			
Mean (SD)	136 (18.1)	133 (18.8)	139 (16.8)
Missing, *N (%)*	147 (0.4%)	90 (0.4%)	57 (0.3%)
DBP (mmHg)			
Mean (SD)	81.6 (10.0)	80.1 (9.96)	83.5 (9.81)
Missing, *N* (%)	147 (0.4%)	90 (0.4%)	57 (0.3%)
HbA1c (mmol/mol)			
Mean (SD)	35.7 (6.36)	35.5 (5.79)	36.1 (6.98)
Missing, *N* (%)	4057 (9.8%)	2384 (10.4%)	1673 (9.0%)
HDL (mmol/L)			
Mean (SD)	1.48 (0.387)	1.63 (0.383)	1.31 (0.312)
Missing, *N* (%)	5080 (12.3%)	2987 (13.0%)	2093 (11.3%)
LDL (mmol/L)			
Mean (SD)	3.54 (0.852)	3.58 (0.851)	3.50 (0.850)
Missing, *N* (%)	3370 (8.1%)	1918 (8.4%)	1452 (7.8%)

SD standard deviation, *N* number, *SBP* systolic blood pressure; diastolic blood pressure, *HbA1c* glycated hemoglobin, *HDL* high-density lipoprotein, *LDL* low-density lipoprotein. Continuous variables were described as the mean (SD), and categorical variables as N (percentage)

retinomics selected for only one disease, among which, fractal dimension and Strahler order of arterial capillary were only selected for hypertension (Additional file 1: Fig. S7).

Improvement in prediction performance after incorporating retinomics

The predictive performance of the baseline and clinical models for the 58 diseases are shown by dots in Fig. 4. The baseline model (including only age and sex) showed moderate predictive performance with a mean C-index of 0.653 (range, 0.551–0.819). Notably, the predictive performance of the baseline model was greatest for the risk of dementia, age-related macular degeneration (AMD), cataract, and Parkinson's disease (C indices > 0.75). The clinical model, which incorporated common risk factors, achieved a mean C-index of 0.697 (range 0.573 to 0.822), demonstrating the highest predictive values for dementia and lung cancer (C-indices > 0.80).

Figure 4 also illustrates how the addition of retinal features improved predictive performance, with purple connecting lines showing the improvement from baseline to retinal model and orange connecting lines indicating the improvement from clinical to full model. Adding retinal features to the baseline model improved the predictive performance, resulting in a mean C-index of 0.693 (range, 0.563–0.832). This represented a mean improvement of 6.42% (range, 1.08–33.18%). The retinal model, using only retinomics with age and sex, achieved a C-index ≥ 0.75 for 13 diseases, encompassing a range of conditions across multiple organ systems. These included cardiovascular diseases (atrial fibrillation, heart failure), neurodegenerative and mental health disorders (Parkinson's disease, dementia, psychoactive substance abuse), ophthalmic conditions (glaucoma, cataract, AMD), fractures, and several cancers (lung cancer, stomach cancer, esophageal cancer, uterine/endometrial cancer). The addition of selected retinomic features to the clinical model improved the predictive performance to a mean C-index of 0.721 (range, 0.576–0.858), with a mean increase of 3.53% (range, 0.50–19.37%). The full model demonstrated optimal performance for predicting uterine/endometrial cancer, lung cancer, dementia, esophageal cancer, chronic obstructive pulmonary disease (COPD), and psychoactive substance abuse (C-indices > 0.8). The C-index values of all models and the relative increase in C-index can be found in Additional file 1: Table S7 and the predictive value of individual retinal features is provided in Additional file 1: Table S8.

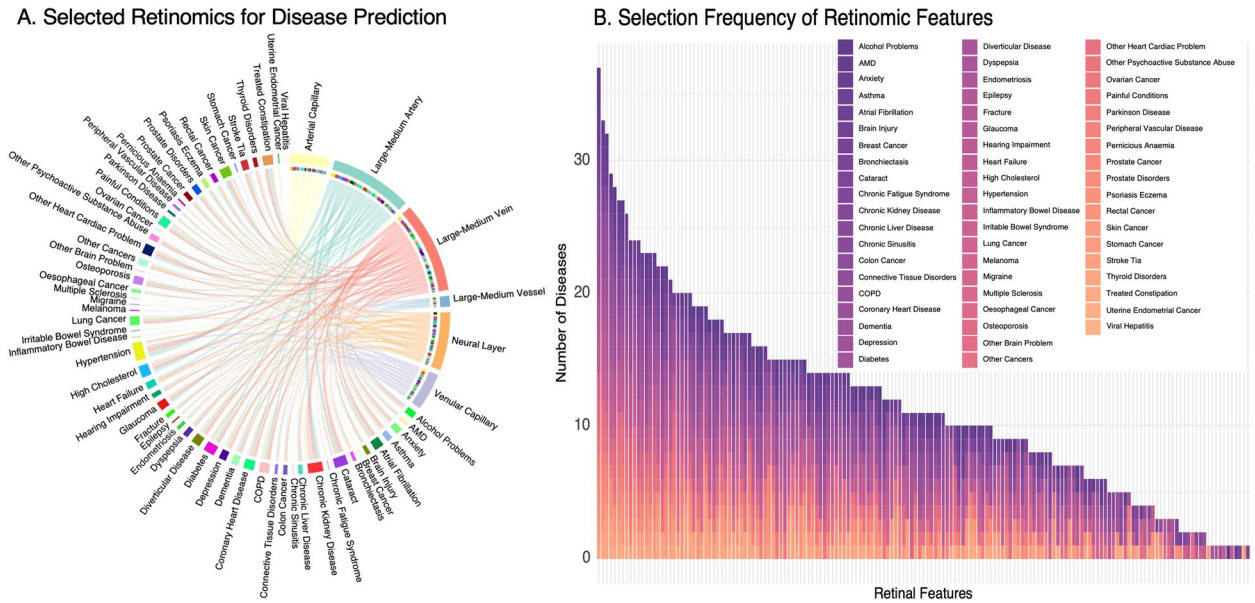

Fig. 3 LASSO-Selected retinomics for disease prediction and selection frequency. **A** Circular diagram showing categories of retinal biomarkers selected by LASSO regression as predictive for specific diseases; connecting lines indicate selection relationships. **B** Bar chart showing the number of diseases associated with each retinal biomarker. Full lists of selected features and corresponding diseases are provided in Additional file 1: Tables S5 (feature-centered view) and S6 (disease-centered view). *LASSO* least absolute shrinkage and selection operator, *COPD* chronic obstructive pulmonary disease, *TIA* transient ischemic attack, *AMD* age-related macular degeneration

Comparison of the screening matrix after incorporating retinomic features

When comparing the retinal model with baseline model, a substantial predictive improvement (> 5% improvement in C-index) with introduction of retinal profiles was found for 24 incident diseases. The LRT test revealed that statistical significance in the improvement for all 24 diseases. When further comparing clinical model and full model, the improvement was over 5% for 12 incident diseases, all statistically significant. Additional file 1: Tables S9–S10 show the result of LRT tests, and Additional file 1: Table S11 shows the results for ICI across four models. Figure 5 presents DR over the FPR ranging from 5 to 40% for those diseases.

In the comparison between baseline and retinal models (Fig. 5A), the retinal model demonstrated an overall trend of superior detection rates compared to the baseline model across all 24 conditions with substantial C-index improvement. The results showed that incorporating retinomic features led constant improvement in DR without introducing more false positive cases, with the exception for ovarian cancer at FPR of 0.2 and viral hepatitis at FPR of 0.25. Among 22 conditions showing consistently higher DR across all FPR levels, when simply using retinomics with age and sex, five conditions had a C-index higher than 0.75, including psychoactive substance abuse, glaucoma, and cancers (lung cancer, esophageal cancer, uterine/endometrial cancer). Similarly, when comparing clinical versus full models (Fig. 5B), the full model also showed a consistent superior performance over the clinical model for 11 out of 12 key diseases, suggesting robust and reliable improvement in predictive capability even after accounting for common clinical factors. Additional file 1: Fig. S8 shows comparison among all models for all 24 diseases.

Discussion

Our study explores the potential of retinal imaging—neurovascular retinomics—as a promising tool for predicting incident chronic diseases, using data from

(See figure on next page.)

Fig. 4 C-index improvement with the introduction of retinomic profiles. The plot shows C-index values for 58 chronic conditions, sorted by full model C-index from highest (top) to lowest (bottom). Teal dots represent the baseline model (age and sex only); purple dots represent the retinal model (baseline model plus selected retinal features from LASSO regression); blue dots represent the clinical model (baseline model plus clinical factors including body mass index, ethnicity, smoking status, alcohol consumption, and physical activity); and orange dots represent the full model (combination of clinical and retinal models). Connecting lines show the improvement from baseline to retinal model (purple lines) and from clinical to full model (orange lines). *LASSO* least absolute shrinkage and selection operator

Fig. 4 (See legend on previous page.)

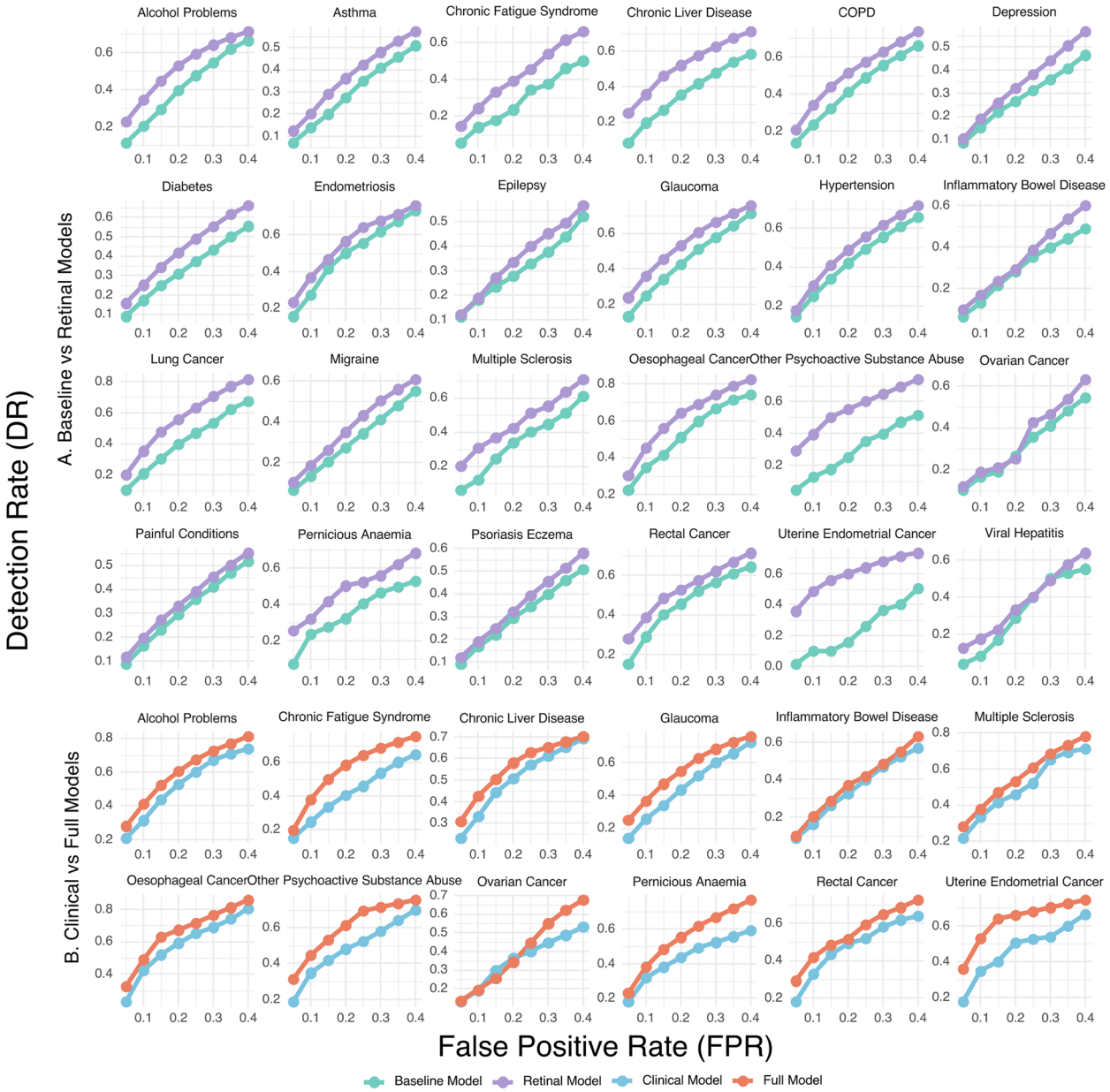

Fig. 5 Detection rate and false positive rate after incorporating retinomics. **A** DR over the FPR ranging from 5 to 40% was presented for both baseline and retinal models. **B** DR over the FPR ranging from 5 to 40% was presented for both clinical and full models. The DR over the FPR ranging from 5 to 40% plot was generated for those diseases where incorporation of retinomics improve the C-index over 5%. *DR* detection rate, *FPR* false positive rate, *C-index* Concordance Index, *COPD* chronic obstructive pulmonary disease. Additional file 1: Fig. S8 shows comparison among all models for all 24 diseases

41,434 UK Biobank participants tracked over a decade. With feature selection, GC-IPL, ISOS-RPE thickness of central subfield, and RPE, and were selected for 37, 33, and 32 diseases, respectively. In addition, retinomics contributed to the universal improvement in the predictive performance, with the mean C-index increased from 0.653 to 0.693 when added to the baseline model and from 0.697 to 0.721 in the clinical model. Notably, retinomics boosted discriminative power by > 5% for 24 diseases in the Baseline Model and 12 in the Clinical Model, while maintaining specificity. Strikingly, a minimalistic model combining retinomics with age/sex achieved robust performance (C-index ≥ 0.75) for 13 conditions, spanning neurodegenerative, cardiovascular, oncologic, and ophthalmic diseases.

GC-IPL, ISOS-RPE thickness of central subfield, and RPE serving as predictors for over 30 distinct diseases. These findings align with the retina's unique window into systemic health, where microvascular integrity and neural tissue reflect cumulative pathological processes. Previous studies explored those features separately and revealed their associations with a variety of systemic conditions. For instance, significant GC-IPL thinning was observed in patients with Alzheimer's disease, mild cognitive impairment, Parkinson's disease, and changes in ISOS-RPE and RPE thickness with diabetes, systemic lupus erythematosus and multiple sclerosis [19–24]. Our study revealed their wide associations with chronic conditions and indicated the potential of these biomarkers further explored as comprehensive health assessment tools.

While introduction of retinomics led to universal improvement in prediction performance, such increase was particularly prominent (exceeding 5%) across 24 conditions when compared with the baseline model. Further analysis on DR across FPR showed that adding retinomics led to consistently higher DR across all FPR levels in 22 conditions. This indicated that adding retinomics increased detection of positive cases without introducing more false positive cases. More importantly, among those 22 conditions, when simply using retinomics with age and sex, five conditions had a C-index higher than 0.75, including psychoactive substance abuse, glaucoma, lung cancer, esophageal cancer, and uterine/endometrial cancer. This demonstrated that adding retinomics not only substantially improved the discriminative power of the predictive models, as evidenced by the enhanced C-indices, but also achieved superior diagnostic efficiency by optimizing the sensitivity–specificity trade-off. This encouraging finding suggests that retinal biomarkers contribute meaningful and specific signal rather than statistical noise to the disease detection paradigm. This favorable performance characteristic would be important prerequisites for population-level screening applications, where minimizing false positives while maintaining high detection sensitivity is crucial for both clinical utility and resource optimization. However, additional validation studies would be needed to establish clinical implementation feasibility.

It should be noted that the retinal model, using only retinomics with age and sex, achieved a C-index ≥ 0.75 for 13 diseases, encompassing cardiovascular diseases (atrial fibrillation, heart failure), neurodegenerative and mental health disorders (Parkinson's disease, dementia, psychoactive substance abuse), ophthalmic conditions (glaucoma, cataract, AMD), fractures, and several cancers (lung cancer, stomach cancer, esophageal cancer, uterine/endometrial cancer). The typical age of presbyopia onset (around 50) naturally brings patients to eye care providers at a life stage when most of those chronic disease risks escalate. This alignment raises the possibility of integrating retinal imaging assessment into routine eye examinations, potentially leveraging existing healthcare touchpoints and infrastructure following evaluation against well-recognized screening frameworks, such as the Wilson–Jungner principles [25].

When added to the clinical model, retinomics led to yield a more than 5% increase in the C-index for 12 conditions, which were all among the above 24 conditions. Apart from ovarian cancer, all conditions had a consistently higher DR across all FPR levels, including psychiatric conditions such as psychoactive substance abuse and alcohol problems, multiple sclerosis, malignancies (esophageal cancer, rectal cancer, and uterine/endometrial cancer), and a cluster of interconnected conditions, including chronic fatigue syndrome and pernicious anemia. These findings underscore the broad applicability of retinomics across a wide range of diseases and highlight its potential as a valuable biomarker, even when integrated with existing Clinical Models that already account for common factors.

Previous studies showed the psychoactive substance abuse can lead to drug-induced retinopathy, with manifestations such as retinal vascular occlusion diseases and toxic optic neuropathy [26], and thinning of RNFL was also observed in terms of retinal measurements [27]. In our study, LASSO feature selection identified 37 retinal parameters with predictive potential for incident substance abuse, including tortuosity, density, and complexity of the vascular network, and INL, GC-IPL, and photoreceptor sublayers. This could be plausibly attributed to the risk factors of psychoactive substance abuse, such as genetic susceptibility, prenatal exposure, and early alcohol and drug use [28, 29]. For instance, a previous study found abnormal retinal tortuosity and optic nerve hypoplasia in children with prenatal alcohol exposure [30]. While some evidence suggests potential retinal associations with substance abuse, the predictive relationship between baseline retinal features and future substance abuse risk remains largely unexplored and requires mechanistic validation. Further research is required to disentangle the retinal profiles of other risk factors of substance abuse.

Previous studies also showed the retinal profiles related to neurodegenerative diseases, including multiple sclerosis (MS) [31–33]. Characterized by axonal loss (demyelination), the retina could show signs of decreased ganglion

cell complex, RNFL thickness, and macular volume [31], decreased vessel density, and reduced macular superficial plexus [32]. In comparison, apart from GC-IPL, we also found tortuosity of arterial capillaries to have increased predictive value of future MS, suggesting that disruptions in both microcirculation and neurodegeneration predate the onset of the disease.

Intriguingly, retinomic profiles also demonstrated increased predictive ability for incident malignancies, such as uterine/endometrial cancer and esophageal cancer. There was scarce evidence on the retina-cancer risk association previously; however, the potential explanation may be exemplified by a recent study showing the association with microvascular dysfunction and incident cancer risk [34]. Oxidative stress was proposed as the common culprit as it leads to endothelial dysfunction and interfering with DNA methylation and genetic instability [34]. Notably, uterine/endometrial cancer is estrogen dependent disorder. Estrogen was found to regulate critical signaling pathways in the retina [35] and a trend narrowing of retinal arterioles and venules were observed with individuals with longer duration of estrogen replacement therapy [36]. However, given the limited prior evidence and indirect mechanistic pathways, these cancer-related findings should be considered exploratory and investigated to establish a mechanistic basis.

For the connection between retina and liver diseases, previous research argued that the combination of hyperammonemia (damaging retinal cells), hypoalbuminemia (altering vascular pressure), and impaired estrogen metabolism, along with portal hypertension, can collectively induce retinal vascular and structural changes detectable through retinal imaging [37]. Our findings extend beyond liver disease to its common complication, anemia, where the predictive value of retinomic profiles was supported by previous studies showing associations between retinal measures (decreased venous tortuosity and reduced central retinal artery equivalent) and anemia [38, 39], and the successful development of deep learning algorithms for hemoglobin prediction [40]. Furthermore, our discovery of retinomic profiles' predictive value for fatigue aligns with the interconnected nature of these conditions, as fatigue often manifests as a compound symptom of both liver disease and anemia, malignancies, or malnutrition from substance abuse [41, 42]. While the retinal-fatigue association appears biologically plausible through these interconnected pathways, further research is needed to validate the predictive utility of retinal biomarkers for fatigue as a standalone condition.

Our study found that retinal imaging shows the potential to enhance risk stratification of multiple chronic diseases. Retinal imaging is widely adopted in clinical practice and is less expensive than other omics technologies. In addition, our results suggested that adding retinomics not only substantially improved the discriminative power of the predictive models but also achieved superior diagnostic efficiency by optimizing the sensitivity–specificity trade-off. Most significantly, using only retinomics with age and sex, a C-index ≥ 0.75 for over a dozen chronic diseases. This temporal convergence between presbyopia-driven eye examinations and peak chronic disease risk creates a potentially valuable screening window. This approach shows the potential to be investigated as a screening tool, particularly in low-resource settings where non-invasive, low-cost, accessible, and simple screening tools are crucial.

However, our study presents some limitations. While our findings are promising, translation to clinical practice would require rigorous evaluation against established screening criteria, including cost-effectiveness analysis, validation of clinical utility through prospective studies, and assessment against Wilson-Jungner principles for population screening programs. Moreover, the varying predictive performance across diseases necessitates focused analysis to identify specific conditions where retinomics offers clinically meaningful improvements and meets decision-making thresholds for practical implementation. Other limitations include the UK Biobank's predominantly White, middle-aged cohort and potential underrepresentation of advanced diseases. Additionally, all retinal images were acquired using the same Topcon device, which may limit generalizability across different imaging platforms. External validation in diverse, high-risk populations using independent datasets from various clinical sites is essential to establish the robustness and clinical applicability of retinomics in real-world settings. Furthermore, with automated retinal image analysis tools, we adopted multiple quality control measures to maximize segmentation and quantification reliability. Nevertheless, exclusion of lower-quality images may introduce selection bias, and measurement variability cannot be entirely eliminated. Despite these limitations, the observed robust improvements in C-index across multiple conditions following LASSO feature selection suggest that biological signal strength exceeded technical measurement noise. Additionally, elucidating causal pathways linking retinal features to systemic diseases—e.g., disentangling substance abuse-related retinal changes from confounding factors like hypertension—warrants further research.

Conclusions

In conclusion, we comprehensively examined neurovascular retinomics as predictors and found added value of the retinomic signatures across a wide spectrum of diseases. Retinal imaging offers advantages as a non-invasive

approach that could potentially leverage existing eye-care infrastructure already frequented by aging populations for presbyopia management (typically from age 50). Its balanced performance with simplicity suggests the potential for preventive healthcare, particularly in resource-limited settings. Future studies validating these biomarkers in diverse populations and evaluating this approach against established screening criteria will be necessary to determine their potential for further practical translation.

Abbreviations

AMD	Age-related macular degeneration
BMI	Body mass index
CFP	Color fundus photography
C-index	Concordance index
COPD	Chronic obstructive pulmonary disease
DBP	Diastolic blood pressure
DR	Detection rate
ELM	External limiting membrane
FPR	False positive rate
GC–IPL	Ganglion cell layer–inner plexiform layer
HbA1c	Glycated hemoglobin
HDL	High-density lipoprotein
ICD	International Classification of Diseases
INL	Inner nuclear layer
ISOS	Inner segment/outer segment
LASSO	Least absolute shrinkage and selection operator
LDL	Low-density lipoprotein
LRT	Likelihood ratio test
MICE	Multiple imputation by chained equations
MS	Multiple sclerosis
OCT	Optical coherence tomography
RPE	Retinal pigment epithelium
RMHAS–FA	Retina-based Microvascular Health Assessment System–Fluorescein Angiography
RNFL	Retinal nerve fiber layer
SBP	Systolic blood pressure
SD	Standard deviation
TIA	Transient ischemic attack
VAD	Vessel area density

Supplementary Information

The online version contains supplementary material available at https://doi.org/10.1186/s12916-025-04450-y.

Additional file 1: Fig. S1. Study design. Fig. S2. C-index improvement with the introduction of CFP profiles. Fig. S3. C-index improvement with the introduction of OCT profiles. Fig. S4. Model performances without LASSO feature selection. Fig. S5. C-index improvement with the introduction of retinomic profiles for 5-year prediction. Fig. S6. C-index improvement with the introduction of retinomic profiles for 10-year prediction. Fig. S7. Retinomics selected for prediction of single disease. Fig. S8. Detection rate and false positive rate for diseases with substantial improvement in prediction performance across models. Table S1. Codes used to identify records of prevalent diseases. Table S2. ICD codes used to identify records of incident diseases. Table S3. Definitions of variables. Table S4. The incidence and median follow-up of diseases. Table S5. The full list of selected retinomics, corresponding diseases, and selection frequency. Table S6. Disease-centred mapping of selected retinomic features. Table S7. C-index values of four models for disease prediction and relative increase after introduction of retinal parameters. Table S8. Predictive value of individual retinal features: C-index improvements over clinical models. Table S9. Likelihood ratio test for retinal model vs baseline model. Table S10. Likelihood ratio test for full model vs clinical model. Table S11. 10-Year Integrated Calibration Indexfor the four models.

Acknowledgements
The Centre for Eye Research Australia receives Operational Infrastructure Support from the Victorian State Government. We thank the InnoHK HKSAR Government for providing valuable supports.

Authors' contributions
Conceptualization, XS, DS and MH; methodology, MB, SJ, DS, and XS; analysis, MY and SJ, manuscript drafting, MY; manuscript review and critical revision, MB, XS, DS, LZ, and MH; visualization, MY and MB; supervision, LZ, XS, DS, and MH. All authors read and approved the final manuscript.

Funding
This work was supported by the Global STEM Professorship Scheme (P0046113), PolyU-Stanford Joint Research Centre for Longitudinal Deep Omics (P0056331) and Henry G. Leong Endowed Professorship in Elderly Vision Health. M.Y. was supported by the Melbourne Research Scholarship established by the University of Melbourne. The funding source had no role in the design and conduct of the study; collection, management, analysis, and interpretation of the data; preparation, review, or approval of the manuscript; and decision to submit the manuscript for publication.

Data availability
The UK Biobank data used in this study are available through the UK Biobank data access procedure (https://www.ukbiobank.ac.uk/). The code used for the retinomics analysis is available through the corresponding author's GitHub repository (https://danli-vision.github.io/). The retinal vascular feature extraction algorithm is publicly available at http://www.retinavessel.com/#/ for testing and analysis.

Declarations

Ethics approval and consent to participate
The UK Biobank study received ethics approval from the North West Multi-Centre Research Ethics Committee (Ref 11/NW/0382) and obtained consent from participants at enrollment.

Consent for publication
Not applicable.

Competing interests
MH and DS hold a patent for A System and a Method for Assessing Health Risk Using Retina Fundus Images (AU 2022903650). The other authors declare that they have no competing interests.

Author details
[1]Centre for Eye Research Australia, Royal Victorian Eye and Ear Hospital, East Melbourne, Australia. [2]Department of Surgery (Ophthalmology), The University of Melbourne, Melbourne, Australia. [3]International Centre for Eye Health, London, School of Hygiene & Tropical Medicine, London, UK. [4]Department of Health Services Research and Policy, London, School of Hygiene & Tropical Medicine, London, UK. [5]Beijing Institute of Ophthalmology, Beijing Tongren Eye Center, Beijing Tongren Hospital, Beijing, China. [6]Guangdong Eye Institute, Department of Ophthalmology, Guangdong Provincial People's Hospital, Guangdong Academy of Medical Sciences, Guangzhou 510080, China. [7]School of Optometry, The Hong Kong Polytechnic University, Kowloon, Hong Kong, SAR, China. [8]Research Centre for SHARP Vision, The Hong Kong Polytechnic University, Kowloon, Hong Kong SAR, China. [9]Centre for Eye and Vision Research (CEVR), 17W Hong Kong Science Park, Hong Kong SAR, China. [10]Department of Epidemiology and Biostatistics, School of Public Health, Xi'an Jiaotong University, Health Science Center, Xi'an, Shaanxi, China. [11]PolyU-Stanford Joint Research Centre for Longitudinal Deep Omics, The Hong Kong Polytechnic University, Kowloon, Hong Kong.

Received: 8 April 2025 Accepted: 13 October 2025
Published online: 27 November 2025

References

1. Yala A, Lehman C, Schuster T, Portnoi T, Barzilay R. A deep learning mammography-based model for improved breast cancer risk prediction. Radiology. 2019;292(1):60–6.
2. Hasin Y, Seldin M, Lusis A. Multi-omics approaches to disease. Genome Biol. 2017;18(1):83.
3. Karczewski KJ, Snyder MP. Integrative omics for health and disease. Nat Rev Genet. 2018;19(5):299–310.
4. Buergel T, Steinfeldt J, Ruyoga G, Pietzner M, Bizzarri D, Vojinovic D, et al. Metabolomic profiles predict individual multidisease outcomes. Nat Med. 2022;28(11):2309–20.
5. Carrasco-Zanini J, Pietzner M, Davitte J, Surendran P, Croteau-Chonka DC, Robins C, et al. Proteomic signatures improve risk prediction for common and rare diseases. Nat Med. 2024;30(9):2489–98.
6. Xie W, Zhao M, Hein TW, Kuo L, Rosa RH Jr. Visualization of retinal blood vessels. Methods Mol Biol. 2021;2319:111–7.
7. Shi D, Zhou Y, He S, Wagner SK, Huang Y, Keane PA, et al. Cross-modality labeling enables noninvasive capillary quantification as a sensitive biomarker for assessing cardiovascular risk. Ophthalmol Sci. 2024;4(3):100441.
8. Yusufu M, Vingrys AJ, Shang X, Zhang L, Shi D, Congdon N, et al. Population-based normative reference for retinal microvascular atlas. Ophthalmol Sci. 2025. https://doi.org/10.1016/j.xops.2025.100723.
9. Yusufu M, Weinreb RN, Kang M, Vingrys AJ, Shang X, Zhang L, et al. Structural and causal links between retinal vascular geometry and neural layer thickness. Microvasc Res. 2025;161:104834.
10. Yusufu M, Friedman DS, Kang M, Padhye A, Shang X, Zhang L, et al. Retinal vascular fingerprints predict incident stroke: findings from the UK biobank cohort study. Heart. 2025. https://doi.org/10.1136/heartjnl-2024-324705.
11. Rothman A, Murphy OC, Fitzgerald KC, Button J, Gordon-Lipkin E, Ratchford JN, et al. Retinal measurements predict 10-year disability in multiple sclerosis. Ann Clin Transl Neurol. 2019;6(2):222–32.
12. Arnould L, Meriaudeau F, Guenancia C, Germanese C, Delcourt C, Kawasaki R, et al. Using artificial intelligence to analyse the retinal vascular network: the future of cardiovascular risk assessment based on oculomics? A narrative review. Ophthalmol Ther. 2023;12(2):657–74.
13. An S, Teo K, McConnell MV, Marshall J, Galloway C, Squirrell D. AI explainability in oculomics: how it works, its role in establishing trust, and what still needs to be addressed. Prog Retin Eye Res. 2025;106:101352.
14. Sudlow C, Gallacher J, Allen N, Beral V, Burton P, Danesh J, et al. UK biobank: an open access resource for identifying the causes of a wide range of complex diseases of middle and old age. PLoS Med. 2015;12(3):e1001779.
15. Chua SYL, Thomas D, Allen N, Lotery A, Desai P, Patel P, et al. Cohort profile: design and methods in the eye and vision consortium of UK Biobank. BMJ Open. 2019;9(2):e025077.
16. Ko F, Foster PJ, Strouthidis NG, Shweikh Y, Yang Q, Reisman CA, et al. Associations with retinal pigment epithelium thickness measures in a large cohort: results from the UK Biobank. Ophthalmology. 2017;124(1):105–17.
17. Shang X, Zhu Z, Zhang X, Huang Y, Zhang X, Liu J, et al. Association of a wide range of chronic diseases and apolipoprotein E4 genotype with subsequent risk of dementia in community-dwelling adults: a retrospective cohort study. eClinicalMedicine. 2022;45:101335.
18. Zekavat SM, Raghu VK, Trinder M, Ye Y, Koyama S, Honigberg MC, et al. Deep learning of the retina enables phenome- and genome-wide analyses of the microvasculature. Circulation. 2022;145(2):134–50.
19. López-de-Eguileta A, Cerveró A, Ruiz de Sabando A, Sánchez-Juan P, Casado A. Ganglion cell layer thinning in Alzheimer's disease. Medicina (Kaunas). 2020;56(10):553.
20. Merten N, Paulsen AJ, Pinto AA, Chen Y, Dillard LK, Fischer ME, et al. Macular ganglion cell-inner plexiform layer as a marker of cognitive and sensory function in midlife. J Gerontol A Biol Sci Med Sci. 2020;75(9):e42–8.
21. Živković M, Dayanir V, Stamenović J, Ljubisavljević S, Pražić A, Zlatanović M, et al. Retinal ganglion cell/inner plexiform layer thickness in patients with Parkinson's disease. Folia Neuropathol. 2017;55(2):168–73.
22. Mititelu M, Uschner D, Doherty L, Bjornstad P, Domalpally A, Drews KL, et al. Retinal thickness and morphology changes on OCT in youth with type 2 diabetes: findings from the TODAY study. Ophthalmol Sci. 2022;2(4):100191.
23. Mehta S, Mehta H. Optical coherence tomography-based diagnosis and monitoring of systemic lupus erythematosus-associated choroidopathy. Cureus. 2022;14(9):e29432.
24. Brandt AU, Oberwahrenbrock T, Ringelstein M, Young KL, Tiede M, Hartung HP, et al. Primary retinal pathology in multiple sclerosis as detected by optical coherence tomography. Brain. 2011;134(Pt 11):e193; author reply e4.
25. Wilson JMG, Jungner G. Principles and practice of screening for disease. Geneva: World Health Organization; 1968.
26. Peragallo J, Biousse V, Newman NJ. Ocular manifestations of drug and alcohol abuse. Curr Opin Ophthalmol. 2013;24(6):566–73.
27. Gemelli H, Fidalgo TM, Gracitelli CPB, de Andrade EP. Retinal nerve fiber layer analysis in cocaine users. Psychiatry Res. 2019;271:226–9.
28. Grant JD, Scherrer JF, Lynskey MT, Lyons MJ, Eisen SA, Tsuang MT, et al. Adolescent alcohol use is a risk factor for adult alcohol and drug dependence: evidence from a twin design. Psychol Med. 2006;36(1):109–18.
29. O'Brien JW, Hill SY. Effects of prenatal alcohol and cigarette exposure on offspring substance use in multiplex, alcohol-dependent families. Alcohol Clin Exp Res. 2014;38(12):2952–61.
30. Tsang TW, Finlay-Jones A, Perry K, Grigg JR, Popova S, Cheung MMY, et al. Eye abnormalities in children with fetal alcohol spectrum disorders: a systematic review. Ophthalmic Epidemiol. 2023;30(4):340–51.
31. Cennamo G, Romano MR, Vecchio EC, Minervino C, della Guardia C, Velotti N, et al. Anatomical and functional retinal changes in multiple sclerosis. Eye. 2016;30(3):456–62.
32. Wang X, Wang X, Chou Y, Ma J, Zhong Y. Significant retinal microvascular impairments in multiple sclerosis assessed through optical coherence tomography angiography. Mult Scler Relat Disord. 2023;70:104505.
33. Jiang Y, Chen Q, Shi D, Miao S, Liu Y, Wang J, et al. Association of retinal microvascular curve tortuosity and multiple sclerosis: a cross-section analysis from the UK Biobank. Mult Scler Relat Disord. 2024;88:105753.
34. Rajai N, Ahmad A, Toya T, Sara JD, Herrmann J, Lerman LO, et al. Coronary microvascular dysfunction is an independent predictor of developing cancer in patients with non-obstructive coronary artery disease. Eur J Prev Cardiol. 2023;30(3):209–16.
35. Hutchinson CV, Walker JA, Davidson C. Oestrogen, ocular function and low-level vision: a review. J Endocrinol. 2014;223(2):R9-18.
36. Wong TY, Knudtson MD, Klein BE, Klein R, Hubbard LD. Estrogen replacement therapy and retinal vascular caliber. Ophthalmology. 2005;112(4):553–8.
37. Xiao W, Huang X, Wang JH, Lin DR, Zhu Y, Chen C, et al. Screening and identifying hepatobiliary diseases through deep learning using ocular images: a prospective, multicentre study. Lancet Digit Health. 2021;3(2):e88–97.
38. Aisen ML, Bacon BR, Goodman AM, Chester EM. Retinal abnormalities associated with anemia. Arch Ophthalmol. 1983;101(7):1049–52.
39. Calli U, Coban F, Evliyaoglu F, Sonmez A. Retinal vascular caliber in patients with newly diagnosed iron deficiency anemia. Photodiagnosis Photodyn Ther. 2022;38:102751.
40. Mitani A, Huang A, Venugopalan S, Corrado GS, Peng L, Webster DR, et al. Detection of anaemia from retinal fundus images via deep learning. Nat Biomed Eng. 2020;4(1):18–27.
41. Sobrero A, Puglisi F, Guglielmi A, Belvedere O, Aprile G, Ramello M, et al. Fatigue: a main component of anemia symptomatology. Semin Oncol. 2001;28(2 Suppl 8):15–8.
42. Bower JE. Cancer-related fatigue—mechanisms, risk factors, and treatments. Nat Rev Clin Oncol. 2014;11(10):597–609.

Publisher's Note